

K-SMPC: Koopman Operator-Based Stochastic Model Predictive Control for Enhanced Lateral Control of Autonomous Vehicles

Jin Sung Kim, *Graduate Student Member, IEEE*, Ying Shuai Quan, *Graduate Student Member, IEEE*, and Chung Choo Chung, *Member, IEEE*

Abstract—This paper proposes Koopman operator-based Stochastic Model Predictive Control (K-SMPC) for enhanced lateral control of autonomous vehicles. The Koopman operator is a linear map representing the nonlinear dynamics in an infinite-dimensional space. Thus, we use the Koopman operator to represent the nonlinear dynamics of a vehicle in dynamic lane-keeping situations. The Extended Dynamic Mode Decomposition (EDMD) method is adopted to approximate the Koopman operator in a finite-dimensional space for practical implementation. We consider the modeling error of the approximated Koopman operator in the EDMD method. Then, we design K-SMPC to tackle the Koopman modeling error, where the error is handled as a probabilistic signal. The recursive feasibility of the proposed method is investigated with an explicit first-step state constraint by computing the robust control invariant set. A high-fidelity vehicle simulator, i.e., CarSim, is used to validate the proposed method with a comparative study. From the results, it is confirmed that the proposed method outperforms other methods in tracking performance. Furthermore, it is observed that the proposed method satisfies the given constraints and is recursively feasible.

Index Terms—Koopman operator, autonomous vehicles, stochastic model predictive control, data-driven control

NOMENCLATURE

- $\{XYZ\}$: Global coordinate frame
- $\{xyz\}$: Local coordinate frame
- $C_{\alpha i}$: Cornering stiffness of tire, $i \in \{f, r\}$
- V_x : Longitudinal speed
- V_y : Lateral speed
- m : Total mass of vehicle
- l_i : Distance between front (rear) tire and center of gravity (CG), $i \in \{f, r\}$
- I_z : Yaw moment of inertia of vehicle
- a_y : Lateral acceleration in $\{xyz\}$
- L : Look-ahead distance
- $e_y = y - y_{des}$: Lateral position error w.r.t. lane
- e_{yL} : Lateral position error on look-ahead point w.r.t. lane

- ψ : Yaw angle of vehicle in global coordinate
- $e_\psi = \psi_{des} - \psi$: Heading angle error in local coordinate w.r.t. lane
- δ : Steering angle
- R : Turning radius
- β : Vehicle side slip angle at CG

I. INTRODUCTION

Autonomous driving vehicles provide advanced driver assistance functions to relieve humans from monotonous long drives and can significantly decrease traffic congestion and accidents. A typical autonomous driving setup comprises essential components such as perception, localization, decision-making, trajectory planning, and control. During trajectory planning and control, knowledge of vehicle dynamics is necessary to execute accurate and safe maneuvers, particularly in complex and unpredictable road environments. Thus, it is essential to have a lateral vehicle dynamic model to design a lateral controller. Lateral control of autonomous driving has gained much attention in many areas, such as automated parking control [1], lateral control on curved roads [2], [3], and automated lane change systems [4]. The bicycle lateral dynamic motion model has been widely used to develop lateral control [5]. In the dynamic model, lateral tire force and acceleration are used to capture the dynamic motion of a vehicle for high-speed driving to represent accurate vehicle behavior. Although many studies have used the bicycle lateral dynamic model, i.e., linear dynamic model, for practical applications under certain conditions, such as a small tire slip angle with a given vehicle speed, the nonlinearity of the vehicle dynamics cannot be ignored because the tire model is highly nonlinear due to the vertical load transfer [6]. Moreover, the vehicle speed is no longer constant in dynamic driving. Therefore, obtaining a model that captures the full vehicle dynamics for various driving conditions is necessary.

Numerous studies have attempted to identify the unknown nonlinear dynamics in different research fields [7]. Recently, a modeling approach based on many datasets has received significant attention for complex systems whose dynamics are difficult to capture [8]. In this context, the Koopman operator has been used in model identification of complex dynamics in recent years. The Koopman operator is a linear map for representing nonlinear systems in an infinite-dimensional space [9]. One of the primary benefits of using the Koopman

Manuscript received XXX, XX, 2023; revised XXX, XX, 2023; accepted XXX, XX, 2023. This work was supported by the National Research Foundation of Korea (NRF) grant funded by the Ministry of Science and ICT (MSIT) (No.2021R1A2C2009908, Data-Driven Optimized Autonomous Driving Technology Using Open Set Classification Method). (*Corresponding author: Chung Choo Chung.*)

Jin Sung Kim, Ying Shuai Quan are with the Dept. of Electrical Engineering, Hanyang University, Seoul 04763, Korea. (e-mail: {jskim06, ysqwan}@hanyang.ac.kr)

Chung Choo Chung is with the Div. of Electrical and Biomedical Engineering, Hanyang University, Seoul 04763, Korea. (+82-2-2220-1724, e-mail: cchung@hanyang.ac.kr)

operator is that the linear model can express the underlying nonlinear behavior. As a result, a linear control design method can be applied to a general nonlinear dynamic system.

In recent years, the Koopman operator-based modeling and control approach has been widely adopted in automated driving because vehicles have highly nonlinear behaviors. In [10]–[14], the authors proposed model identification of nonlinear vehicle dynamics to control vehicle lateral and/or longitudinal velocity. In [15] and [16], the authors considered the global position control of the vehicle. Position control is essential for controlling vehicles properly on roads. In [17], the authors considered the local position with respect to the given trajectory. Then, a mini-sized car was used to show the effectiveness of the proposed system. For practical implementation of the Koopman operator, the papers mentioned above used Extended Dynamic Mode Decomposition (EDMD) or neural networks to approximate the Koopman operator in a finite-dimensional space. Unfortunately, the approximated Koopman operator causes approximation uncertainty, which results in the presence of modeling errors because there is a residual term in the optimization problem of approximation of the Koopman operator [18]–[20]. Therefore, the model mismatch can not be negligible in using the Koopman operator, even though the Koopman operator has a powerful linear property representing the nonlinear dynamics. To tackle this problem, [21] proposes a method of handling the approximation error with an estimator. In [19] and [22], the authors design Robust Model Predictive Control (RMPC) for the nonlinear system with constraints satisfaction under uncertainties. However, it is challenging to obtain a robust positively invariant set against the uncertainties of the approximated Koopman operator. Moreover, an RMPC scheme is conservative since the worst-case of uncertainties is considered [23], [24].

In this context, this paper proposes a Koopman operator-based stochastic MPC (K-SMPC) for enhanced lateral control of autonomous vehicles. The EDMD method is adopted to obtain the approximated Koopman operator in a finite-dimensional space for practical use of the Koopman operator. Our work considers the modeling error due to the EDMD-based finite-dimensional approximation of the Koopman operator. We handle the modeling error as a probabilistic signal and design the SMPC to tackle the error. As a result, the proposed method is less conservative than the RMPC. To our knowledge, this paper is the first research in which the SMPC is used to resolve the modeling error of the approximated Koopman operator in the LKS application. All constraints are satisfied under the Koopman modeling error with recursive feasibility in the proposed method. A high-fidelity vehicle simulator, CarSim, is used to validate the proposed method. The simulation results confirmed that the proposed method always satisfies the constraints and is recursively feasible. Moreover, a comparative study shows that the proposed method outperforms other methods: the linear vehicle model-based SMPC (L-SMPC) and the Koopman-based Linear Quadratic Regulator (K-LQ) [25]. The contributions of the paper are three-fold:

- We compute the Koopman-based vehicle model for the Lane Keeping System (LKS). The vehicle model has highly nonlinear dynamic motion in dynamic driving,

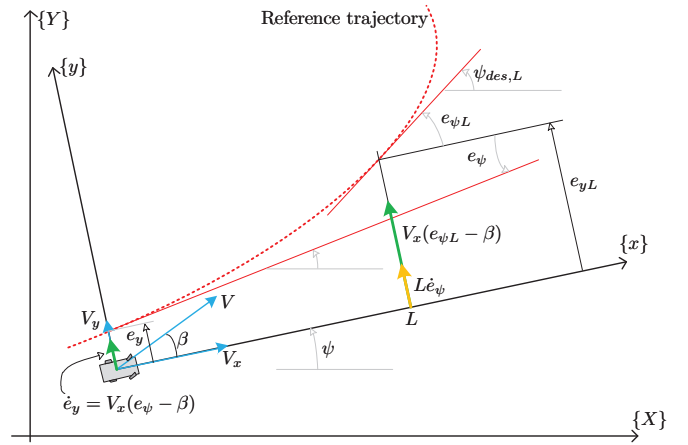


Fig. 1. Look-ahead lateral dynamic model [26]

such as varying vehicle speed or cornering stiffness. Thus, we reformulate the Koopman-based vehicle model from [25] to effectively capture the vehicle nonlinear dynamics for the LKS in various driving situations.

- Uncertainty of the approximated Koopman operator is considered and handled by the probabilistic constraints of K-SMPC. Since the approximated Koopman model may fail to represent the system accurately, we designed K-SMPC to predict the expected state of the system. With the proposed algorithm, we generated K-SMPC resistant to error in the model identification and randomness in the dynamics.
- We prove the recursive feasibility of the proposed K-SMPC with an explicit first-step state constraint by computing a robust control invariant set by providing a theorem. Compared to a mixed worst-case/stochastic prediction for constraint tightening, the proposed method is less conservative but has recursive feasibility.

The rest of the paper is structured as follows: Section II investigates the vehicle nonlinear dynamics. Section III introduces the background of the Koopman operator theory and its application to vehicle dynamics for the LKS. Based on the obtained Koopman operator, Section IV presents the SMPC design process with recursive feasibility. The simulation results are shown in Section V, and the conclusion of the paper is described in Section VI.

II. NONLINEAR VEHICLE DYNAMICS ON ROADS

A. Clothoid Road Lane Model

We introduce a road lane where a vehicle may run to be represented by a cubic polynomial curve. The cubic polynomial curve is defined by the clothoid curve, where the curvature of the curve is continuous and slowly varying [3], [26]. To consider the clothoid constraint with slowly varying curvature κ , it can be defined as

$$\kappa(s) = 2C_2 + 6C_3s, \quad (1)$$

where s denotes the arc length, $2C_2$ denotes the curvature at $s = 0$, and $6C_3$ denotes the curvature rate. For a small

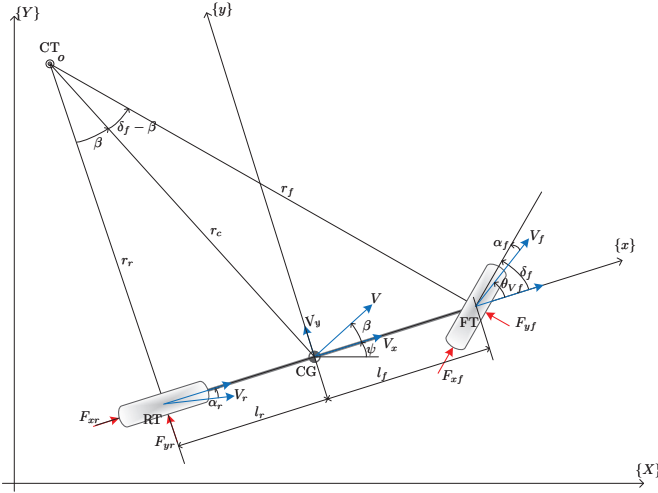


Fig. 2. Single track bicycle model

curvature, the arc length s can be approximated by the longitudinal distance x [5]. Then, integrating (1) twice leads to a clothoid cubic polynomial road model such that

$$f(x) = C_0 + C_1x + C_2x^2 + C_3x^3, \quad (2)$$

where C_0 denotes the lateral offset, and C_1 denotes the heading angle error. In general, the lane curve model is widely applied with the assumption of a plain road in a camera-based lane recognition (see [27] and references therein). It is well known that the road model is obtained by a camera sensor. Moreover, from (1), C_2 and C_3 are the shape of the road, which is not dependent on the vehicle motion. On the other hand, C_0 and C_1 in (2) are dependent on the vehicle motion since they show the relationship between the vehicle and the road lane curve.

This paper considers the look-ahead distance to mimic human driving behavior [28]. By using (2), the heading angle error and a lateral offset at look-ahead distance L can be computed as

$$\begin{aligned} f(L) = e_{yL} &= C_0 + C_1L + C_2L^2 + C_3L^3, \\ f'(L) = e_{\psi L} &= C_1 + 2C_2L + 3C_3L^2, \end{aligned} \quad (3)$$

as shown in Fig. 1.

B. Lateral Vehicle Motion Model

In this subsection, we derive the lateral vehicle motion model as the nonlinear dynamics. To begin with, consider Newton's second law in the lateral direction of the vehicle such that

$$ma_y = F_{yf} + F_{yr} \quad (4)$$

where a_y is the lateral acceleration of the vehicle at the center of gravity and F_{yf} and F_{yr} are the lateral tire forces at the front and rear wheels, respectively. The lateral tire force can

be represented as a nonlinear function with respect to the tire slip angle α_f , α_r , and the vehicle state, which is given by

$$\begin{aligned} F_{yf} &= 2C_{\alpha f}(\alpha_f) \cdot \left(\delta - \arctan\left(\frac{V_y + l_f\dot{\psi}}{V_x}\right) \right), \\ F_{yr} &= 2C_{\alpha r}(\alpha_r) \cdot \left(-\arctan\left(\frac{V_y - l_r\dot{\psi}}{V_x}\right) \right), \end{aligned} \quad (5)$$

where $C_{\alpha f}$ is the cornering stiffness which is a function of the tire slip angle. There are two terms contributing to the lateral acceleration: the translational acceleration \ddot{y} , and the centripetal acceleration $V_x\dot{\psi}$ such that

$$a_y = \ddot{y} + V_x\dot{\psi}. \quad (6)$$

Substituting (4) into (6) leads to

$$\ddot{y} = -V_x\dot{\psi} + \frac{F_{yf} + F_{yr}}{m}. \quad (7)$$

In addition, the yaw dynamics of the vehicle along the z-axis are represented by

$$I_z\ddot{\psi} = l_fF_{yf} - l_rF_{yr}, \quad (8)$$

where l_f and l_r are the distances of the front wheel and the rear wheel from the center of gravity, respectively.

Let us obtain the heading angle error rate

$$\dot{e}_{\psi} = \dot{\psi}_{des} - \dot{\psi}, \quad (9)$$

and the lateral position error rate

$$\dot{e}_y = \dot{y} - \dot{y}_{des} = \dot{y} + V_x e_{\psi}. \quad (10)$$

Then, we can obtain

$$\begin{aligned} \ddot{e}_y &= \ddot{y} - \ddot{y}_{des} = \ddot{y} + V_x\dot{e}_{\psi} \\ &= -V_x\dot{\psi} + \frac{F_{yf} + F_{yr}}{m} + V_x\dot{e}_{\psi}. \end{aligned} \quad (11)$$

In order to mimic the general behavior of expert drivers, it is necessary to consider error at the look-ahead distance [29], as shown in Fig. 1. Then, the lateral offset error at the look-ahead distance is given by

$$\begin{aligned} \dot{e}_{yL} &= V_x(e_{\psi L} - \beta) + L\dot{e}_{\psi} \\ &= \dot{e}_y - L\dot{\psi} + V_x(e_{\psi L} - e_{\psi}) + L\dot{\psi}_{des}. \end{aligned} \quad (12)$$

Now, let us define the state, the input, and the external signal of the vehicle dynamics [25], [29], [30]

$$\begin{aligned} \mathbf{x} &= [e_y \quad e_{yL} \quad \dot{e}_y \quad e_{\psi} \quad \dot{\psi} \quad a_y \quad V_y]^T, \\ \mathbf{u} &= \delta, \\ \varphi &= [V_x \quad C_2 \quad C_3]^T, \end{aligned} \quad (13)$$

where $\mathbf{x} \in \mathbb{R}^n$, $\mathbf{u} \in \mathbb{R}^m$, and $\varphi \in \mathbb{R}^d$. Then, we can describe the nonlinear vehicle dynamics such that

$$\dot{\mathbf{x}} = f_v(\mathbf{x}, \mathbf{u}, \varphi). \quad (14)$$

Since the lateral tire force (5) is highly nonlinear with respect to the tire slip angle and vehicle motion, (14) can be represented as a nonlinear structure. Then, discretizing (14) leads to a discrete-time vehicle nonlinear model given by

$$\mathbf{x}_{k+1} = f_d(\mathbf{x}_k, \mathbf{u}_k, \varphi_k). \quad (15)$$

As reported in [5], the vehicle dynamics have strong couplings in lateral and longitudinal directions due to the tire characteristics. Thus, it can be challenging to identify the cornering stiffness parameters. Here, this paper tackles this nonlinearity of the vehicle dynamics by taking advantage of an emerging technique in the field of data-driven modeling, i.e., the Koopman operator theory. It is not necessary to have any prior knowledge of the internal parameters of the vehicle. Only the collected dataset of the system state and input are required to obtain the Koopman operator. Using the property of the Koopman operator, we construct a linear vehicle dynamic model precisely representing (15) in a lifted space. We will discuss the detailed design process in the following sections.

III. KOOPMAN OPERATOR

A. Preliminary

The Koopman operator was initially proposed to capture the nonlinear autonomous dynamics in an infinite-dimensional space [9]. Thus, let us consider the discrete-time nonlinear autonomous dynamics such that

$$\boldsymbol{\eta}_{k+1} = f_a(\boldsymbol{\eta}_k), \quad (16)$$

where $\boldsymbol{\eta}_k \in \mathcal{N}$ is the state of the system, f_a is the nonlinear map, and $k \in \mathbb{Z}_+$ is the discrete-time. Let us consider a real-valued scalar function $\pi_a : \mathcal{N} \rightarrow \mathbb{R}$, which is the so-called *observable* [7], [31]. Each function π_a is an element of an infinite-dimensional function space \mathcal{F}_a (i.e., $\pi_a \in \mathcal{F}_a$) [31]. Then, the Koopman theory provides an alternative representation of (16) by a linear operator, i.e., the Koopman operator $\mathcal{K}_a : \mathcal{F}_a \rightarrow \mathcal{F}_a$ in the space \mathcal{F}_a such that

$$\mathcal{K}_a \pi_a(\boldsymbol{\eta}_k) = \pi_a(f_a(\boldsymbol{\eta}_k)) \quad (17)$$

for every $\pi_a \in \mathcal{F}_a$, where the function space \mathcal{F}_a is invariant under the Koopman operator [18], [31].

There are several ways to apply the Koopman operator to controlled nonlinear systems with a slight change [18], [32], [33]. This paper adopts the data-driven method from [18], which is a rigorous and practical approach. Let us consider a controlled discrete-time nonlinear system such that

$$\boldsymbol{\eta}_{k+1} = f(\boldsymbol{\eta}_k, \boldsymbol{\nu}_k), \quad (18)$$

where $\boldsymbol{\nu}_k \in \mathcal{V}$ is the system input. We can then define the extended state-space $\mathcal{N} \times \mathcal{I}(\mathcal{V})$, where $\mathcal{I}(\mathcal{V})$ is the space of all the control sequences, $\boldsymbol{\mu} := (\boldsymbol{\nu}_k)_{k=0}^{\infty}$. Using the scheme from [18], we can define the extended state given by

$$\chi = \begin{bmatrix} \boldsymbol{\eta} \\ \boldsymbol{\mu} \end{bmatrix}. \quad (19)$$

With the extended state (19), (18) can be in the form of an autonomous system such that

$$\chi_{k+1} = F(\chi_k) := \begin{bmatrix} f(\boldsymbol{\eta}_k, \boldsymbol{\mu}_k(0)) \\ \mathcal{L}\boldsymbol{\mu}_k \end{bmatrix}, \quad (20)$$

where \mathcal{L} is the left shift operator, i.e., $\mathcal{L}\boldsymbol{\mu}_k = \boldsymbol{\mu}_{k+1}$, and $\boldsymbol{\mu}_k(0) = \boldsymbol{\nu}_k$ is the first element of the control sequence of

$\boldsymbol{\mu}$ at the time step k [18]. Now, we can define the Koopman operator $\mathcal{K}_f : \mathcal{F} \rightarrow \mathcal{F}$ for (20) as

$$\mathcal{K}_f \pi(\chi_k) = \pi(F(\chi_k)), \quad (21)$$

where $\pi : \mathcal{N} \times \mathcal{I}(\mathcal{V}) \rightarrow \mathbb{R}$ is a real-valued function, which belongs to the extended function space \mathcal{F} [31]. Interestingly, it is observed that the Koopman operator is linear in the function space \mathcal{F} , even though the dynamical system is nonlinear [31].

B. Koopman Operator-based Vehicle Modeling

In this subsection, we introduce the Koopman operator-based vehicle modeling approach. In (21), we can see that the Koopman operator \mathcal{K}_f lies in the infinite-dimensional space for representing the original nonlinear dynamics [9], [31]. Thus, it is challenging to directly use the Koopman operator if the finite-dimensional approximation of the Koopman operator is not obtained. To resolve this problem, this paper uses the EDMD method from [18], [34]. Let us first recall the state, the control input, and the external signal of the vehicle dynamics (15) such that

$$\begin{aligned} \mathbf{x} &= [e_y \quad e_{yL} \quad \dot{e}_y \quad e_\psi \quad \dot{\psi} \quad a_y \quad V_y]^T, \\ \mathbf{u} &= \delta, \\ \varphi &= [V_x \quad C_2 \quad C_3]^T. \end{aligned} \quad (22)$$

Remark 1. *Since this paper focuses on vehicle modeling for lateral motion control, the longitudinal speed V_x can be the external signal. In addition, the curvature and curvature rate of the road lane, i.e., C_2 and C_3 , is independent of the vehicle state, as mentioned in Subsection II-A [25], [29]. Thus, C_2 and C_3 can be the external signal. In general, φ is available with an in-vehicle sensor and a camera.* \diamond

Then, we take and modify the approach from [18], [34] to define the extended state given by

$$\mathcal{X}_k = \begin{bmatrix} \mathbf{x}_k \\ \mathbf{u}_k \\ \varphi_k \end{bmatrix}, \quad (23)$$

where $\mathcal{X}_k \in \mathbb{R}^{n+m+d}$ is the extended state. Then, we can have the discrete-time autonomous system for the extended state such that

$$\mathcal{X}_{k+1} = F(\mathcal{X}_k) := \begin{bmatrix} f_d(\mathbf{x}_k, \mathbf{u}_k, \varphi_k) \\ \mathbf{u}_{k+1} \\ \varphi_{k+1} \end{bmatrix}. \quad (24)$$

The Koopman operator can then be obtained by

$$\mathcal{K}\boldsymbol{\xi}(\mathcal{X}_k) = \boldsymbol{\xi}(F(\mathcal{X}_k)), \quad (25)$$

where $\boldsymbol{\xi}(\mathbf{x}_k, \mathbf{u}_k, \varphi_k) = [\phi(\mathbf{x}_k) \quad \mathbf{u}_k \quad \mathbf{w}_k]^T$ is the lifting function. In this case, we consider $\phi(\mathbf{x}_k)$ as

$$\phi(\mathbf{x}_k) = \begin{bmatrix} \phi_1(\mathbf{x}_k) \\ \phi_2(\mathbf{x}_k) \\ \vdots \\ \phi_N(\mathbf{x}_k) \end{bmatrix} \in \mathbb{R}^N, \quad (26)$$

where $\phi_i : \mathbb{R}^n \rightarrow \mathbb{R}$ is the real-valued lifting function, and $N \gg n$. In general, the lifting function ϕ_i is a user-defined

nonlinear function. In this paper, the EDMD method from [18] is used to approximate the Koopman operator in (25) as a finite-dimensional linear operator. The analytical solution is obtained by

$$\min_{\mathcal{K}} \sum_{i=0}^{M-1} \|\xi(\mathcal{X}_{i+1}) - \mathcal{K}\xi(\mathcal{X}_i)\|_2^2, \quad (27)$$

where M is the length of a dataset. To solve the optimization problem, we first need to collect a dataset by conducting several numerical simulations. Then the dataset matrices are given as

$$\begin{aligned} \mathbf{X} &= [\mathbf{x}_0 \ \mathbf{x}_1 \ \dots \ \mathbf{x}_{M-1}] \in \mathbb{R}^{n \times M}, \\ \mathbf{U} &= [\mathbf{u}_0 \ \mathbf{u}_1 \ \dots \ \mathbf{u}_{M-1}] \in \mathbb{R}^{m \times M}, \\ \mathbf{D} &= [\varphi_0 \ \varphi_1 \ \dots \ \varphi_{M-1}] \in \mathbb{R}^{d \times M}, \\ \mathbf{Y} &= [\mathbf{x}_1 \ \mathbf{x}_2 \ \dots \ \mathbf{x}_M] \in \mathbb{R}^{n \times M}, \end{aligned} \quad (28)$$

where M is the length of a dataset. Let us define the basis function ϕ_i such that

$$\mathbf{z}_k = \phi(\mathbf{x}_k) := \begin{bmatrix} \mathbf{x}_k \\ \phi_{N-n}(\mathbf{x}_k) \\ \vdots \\ \phi_N(\mathbf{x}_k) \end{bmatrix} \in \mathbb{R}^N. \quad (29)$$

Since predicting the future input and external signal is not of interest [18], [20], this paper omits the last $(m+d)$ rows of each $\xi(\mathcal{X}_{i+1}) - \mathcal{K}\xi(\mathcal{X}_i)$ in (27). However, we focus on the first N rows such that

$$\min_{\mathcal{K}} \sum_{i=0}^{M-1} \left\| \begin{bmatrix} \phi(\mathbf{x}_{k+1}) \\ \mathbf{u}_{k+1} \\ \varphi_{k+1} \end{bmatrix} - \mathcal{K} \begin{bmatrix} \phi(\mathbf{x}_k) \\ \mathbf{u}_k \\ \varphi_k \end{bmatrix} \right\|_2^2 \quad (30)$$

where

$$\mathcal{K} = \begin{bmatrix} A & B & B_\varphi \\ (*) & (*) & (*) \\ (*) & (*) & (*) \end{bmatrix}.$$

Then, (27) can be converted into

$$\min_{A, B, B_\varphi} \|\tilde{\mathbf{Y}} - A\tilde{\mathbf{X}} - B\mathbf{U} - B_\varphi\mathbf{D}\|_F^2, \quad (31)$$

where

$$\begin{aligned} \tilde{\mathbf{X}} &= [\phi(\mathbf{x}_0) \ \phi(\mathbf{x}_1) \ \dots \ \phi(\mathbf{x}_{M-1})], \\ \tilde{\mathbf{Y}} &= [\phi(\mathbf{x}_1) \ \phi(\mathbf{x}_2) \ \dots \ \phi(\mathbf{x}_M)], \end{aligned}$$

and $\|\cdot\|_F$ is the Frobenius norm. By solving the optimization problem (31) [18], [25], we can obtain the linear model such that

$$\begin{aligned} \mathbf{z}_{k+1} &= A\mathbf{z}_k + B\mathbf{u}_k + B_\varphi\varphi_k + G\mathbf{w}_k, \\ \mathbf{x}_k &= C\mathbf{z}_k. \end{aligned} \quad (32)$$

where the reconstruction matrix C is obtained by $C = [\mathbf{I}_{(n \times n)} \ \mathbf{0}]$. Here, note that this paper introduces the residual term \mathbf{w}_k in (32). This is because there may be a residual term in solving (31), which results in the approximation error of the Koopman operator [18]–[20]. Thus, the modeling error of the tuple (A, B, B_φ) is inevitable due to the approximated Koopman operator in a finite-dimensional space. To resolve the problem, we consider the residual term \mathbf{w}_k of the

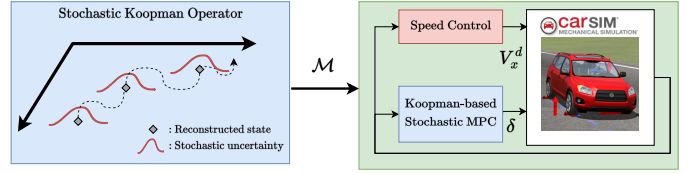


Fig. 3. Schematic illustration of the proposed method. The approximation error of the Koopman operator is handled as a stochastic uncertainty.

Koopman-based model in designing the controller. Moreover, we assume that \mathbf{w}_k is the bounded probabilistic signal such that $\mathbf{w}_k \in \mathcal{W} = \{\mathbf{w}_k \mid \|\mathbf{w}_k\|_\infty \leq \bar{\mathbf{w}}\}$, $\mathbb{E}[\mathbf{w}_k] = \mathbf{0}$, and the covariance matrix of \mathbf{w}_k is $\Sigma_{\mathbf{w}}$. In the following subsection, we will introduce the design process of the proposed controller considering the approximation error \mathbf{w}_k .

IV. KOOPMAN OPERATOR-BASED STOCHASTIC MODEL PREDICTIVE CONTROL

A. System State, Objective, and Constraints

In this subsection, we first describe the system state to be controlled. One can denote the predicted trajectories with $k+i|k$, i.e., predicted at time k and i steps into the future. We define $\mathbf{z}_{k+i|k}$ as

$$\mathbf{z}_{k+i|k} = \mathbf{s}_{k+i|k} + \mathbf{e}_{k+i|k}, \quad (33)$$

where the state $\mathbf{z}_{k+i|k}$ is decomposed into two parts: the deterministic state $\mathbf{s}_{k+i|k}$ and the zero mean stochastic error $\mathbf{e}_{k+i|k}$, i.e., $\mathbb{E}[\mathbf{z}_{k+i|k}] = \mathbf{s}_{k+i|k}$. Let us define the stabilizing control gain K satisfying the following Riccati equation such that

$$P = A^T P A - A^T P B (R + B^T P B)^{-1} B^T P A + Q \quad (34)$$

where $K = (R + B^T P B)^{-1} B^T P A$. Then, as it is common in the linear SMPC scheme, e.g., [23], the control strategy is given by

$$\mathbf{u}_{k+i|k} = K\mathbf{z}_{k+i|k} + \mathbf{v}_{k+i|k} \quad (35)$$

where $\mathbf{v}_{k+i|k} \in \mathbb{R}^m$ is the optimal control input obtained by solving the SMPC problem. Using (33) and (35), one can derive the dynamics of the deterministic state and error state given by

$$\mathbf{s}_{k+i+1|k} = A_{cl}\mathbf{s}_{k+i|k} + B\mathbf{v}_{k+i|k} + B_\varphi\varphi_{k+i|k} \quad (36a)$$

$$\mathbf{e}_{k+i+1|k} = A_{cl}\mathbf{e}_{k+i|k} + G\mathbf{w}_{k+i|k} \quad (36b)$$

where $A_{cl} = A - BK$ is strictly stable.

Remark 2. As mentioned in II-A, C_2 and C_3 are intrinsic parameters of a road shape independent of the vehicle's lateral motion [5]. Thus, with a given road, it is immediate to obtain C_2 and C_3 in the prediction horizon [35]. Moreover, the vehicle speed can be obtained with speed planning and control according to the road curvature [2]. Therefore, this paper assumes that φ is available in the horizon N . \diamond

Let the cost function in a stochastic framework be

$$\mathcal{J} = \mathbb{E} \left[\sum_{i=0}^{N_p-1} \left(\mathbf{z}_{k+i|k}^T Q_{xx} \mathbf{z}_{k+i|k} + \mathbf{z}_{k+i|k}^T Q_{xv} \mathbf{v}_{k+i|k} + \mathbf{v}_{k+i|k}^T Q_{vv} \mathbf{v}_{k+i|k} \right) + \mathbf{z}_{N_p|k}^T P \mathbf{z}_{N_p|k} \right], \quad (37)$$

where $\mathbb{E}[\cdot]$ denotes the expectation value, $Q_{xx} \succeq 0$, $Q_{xv} \succeq 0$, $Q_{vv} \succ 0$, and P is the solution to (34). Substituting (33) into (37) leads to the cost function in a deterministic framework by using $\mathbb{E}[\mathbf{z}_{k+i|k}] = \mathbf{s}_{k+i|k}$ such that

$$\mathcal{J} = \sum_{i=0}^{N_p-1} \left(\mathbf{s}_{k+i|k}^T Q_{xx} \mathbf{s}_{k+i|k} + \mathbf{s}_{k+i|k}^T Q_{xv} \mathbf{v}_{k+i|k} + \mathbf{v}_{k+i|k}^T Q_{vv} \mathbf{v}_{k+i|k} \right) + \mathbf{s}_{k+N_p|k}^T P \mathbf{s}_{k+N_p|k} + c, \quad (38)$$

where $c = \mathbb{E}[\sum_{i=0}^{N_p-1} (\mathbf{e}_{k+i|k}^T Q_{xx} \mathbf{e}_{k+i|k}) + \mathbf{e}_{N_p|k}^T P \mathbf{e}_{N_p|k}]$ which does not depend on the decision variables $\mathbf{v}_{k+i|k}$. Thus, we can convert the stochastic cost function into the deterministic cost function.

In terms of the stochastic error and its influence on the deterministic state, the state constraints at the i -th time step in the receding horizon can be described as probabilistic constraints based on the risk level or allowable probability of violation, i.e., $\epsilon_i \in [0, 1]$, such that

$$\mathcal{P}[H_i \mathbf{z}_{k+i|k} \leq h_i] \geq 1 - \epsilon_i, \quad (39)$$

where $\mathcal{P}[\cdot]$ denotes the probability, $H_i \in \mathbb{R}^{p \times N}$, and $h_i \in \mathbb{R}^p$. Then, the following theorem provides the process to convert (39) into the deterministic constraints.

Theorem 1. *At time k with a given prediction horizon N_p , the probabilistic constraints of (39) are satisfied if and only if the following deterministic constraints are satisfied such that*

$$H_i \mathbf{s}_{k+i|k} \leq h_i - q_i(1 - \epsilon_i), \text{ for } i = 0, \dots, N_p - 1 \quad (40)$$

where $q_i(1 - \epsilon_i) = \sqrt{H_i^T \Sigma_i H_i} \sqrt{\frac{1 - \epsilon_i}{\epsilon_i}}$. \diamond

Proof. By using (33), we can rewrite (39) as

$$\mathcal{P}[H_i \mathbf{s}_{k+i|k} \leq h_i - H_i \mathbf{e}_{k+i|k}] \geq 1 - \epsilon_i. \quad (41)$$

Then, we can obtain

$$H_i \mathbf{s}_{k+i|k} \leq h_i - q_i(1 - \epsilon_i) \quad (42)$$

where $\mathcal{P}[-q_i(1 - \epsilon_i) \leq -H_i \mathbf{e}_{k+i|k}] = 1 - \epsilon_i$ because $\mathbf{s}_{k+i|k}$ is the deterministic variable. Then, it is immediate to derive $q_i(1 - \epsilon_i) = \sqrt{H_i^T \Sigma_i H_i} \sqrt{\frac{1 - \epsilon_i}{\epsilon_i}}$ by Chebyshev–Cantelli Inequality [36], where $\Sigma_{i+1} = A_{cl}^T \Sigma_i A_{cl} + G^T \Sigma_w G$ with $\Sigma_0 = \Sigma_w$. \square

Consequently, we can define the sets of the deterministic state constraints and input hard constraints for the K-SMPC as

$$\mathcal{S} = \{\mathbf{s}_{k+i|k} \in \mathbb{R}^N \mid H_i \mathbf{s}_{k+i|k} \leq h_i - q_i(1 - \epsilon_i)\}, \quad (43a)$$

$$\mathcal{U} = \{\mathbf{u}_{k+i|k} \in \mathbb{R}^m \mid \underline{\mathbf{u}} \leq \mathbf{u}_{k+i|k} \leq \bar{\mathbf{u}}\}, \quad (43b)$$

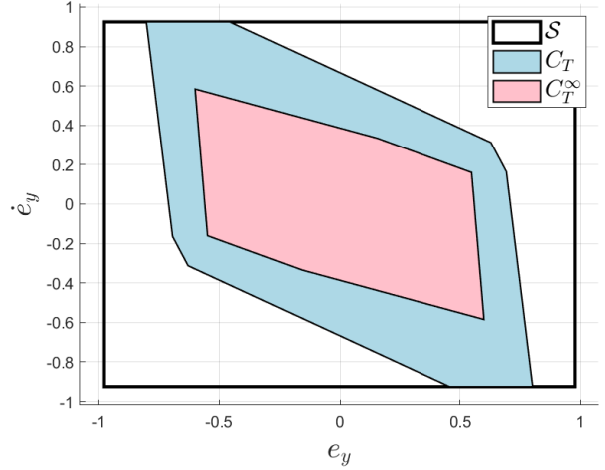


Fig. 4. Recursive set projected on the space of the first and third state of \mathbf{s}_k .

where $\underline{\mathbf{u}}$, and $\bar{\mathbf{u}}$ denote the lower bound, and the upper bound, respectively. Moreover, a constraint tightening method similar to (42) can be applied to define the terminal region such that

$$\mathcal{S}_f = \{\mathbf{s}_{k+N_p|k} \in \mathbb{R}^N \mid H_N \mathbf{s}_{k+N_p|k} \leq h_{N_p} - q_N(1 - \epsilon_{N_p})\}. \quad (44)$$

B. Recursive Feasibility and Stability of Resulting K-SMPC Algorithm

In order to guarantee the recursive feasibility of the K-SMPC, we construct the first-step state constraint of the prediction horizon [37]. In [38], it was reported that the probability of the constraint satisfaction in i steps of the prediction horizon at time k is not equal to the probability of the constraint satisfaction in $i - 1$ steps of the prediction horizon at time $k + 1$. Thus, we need to use further constraints to satisfy the recursive feasibility. In [38], the authors proposed a mixing stochastic and worst-case state prediction in constraint tightening for recursive feasibility in the presence of perturbation. However, in [39], the authors point out the mixed stochastic/worst-case approach is rather restrictive and has higher average costs if the solution is near a chance constraint. Instead, [39] proposed the constraint only in the first step of the prediction horizon where only the recursive feasibility is of interest. Therefore, we focus on the first step state constraint for recursive feasibility, proposed by a paper in the model-based setting [37]. Thus, the proposed method is less conservative than the mixed-state prediction approach, e.g., [38].

Let us define the following set

$$C_T = \left\{ \begin{array}{l} \mathbf{s}_{0|k} \in \mathbb{R}^N \\ \exists \mathbf{v}_{0|k}, \dots, \mathbf{v}_{N_p-1|k} \\ (36a) \text{ and } (43) \text{ hold} \\ \mathbf{s}_{k+N_p|k} \in \mathcal{S}_f \end{array} \right\}$$

as the T -step set with a feasible first step state constraint for the deterministic system (36a) under tightened constraints. The T -step set is obtained by the backward recursion from [40]. Since C_T is not necessarily robust positively invariant with respect to the disturbance set \mathcal{W} , further computation of the

robust control invariant polytope C_T^∞ is required. To calculate C_T^∞ , let us define a set as

$$C_T^{i+1} = \left\{ \mathbf{s} \in C_T^i \mid \begin{array}{l} \exists v_{0|k} \text{ such that (43b) holds,} \\ \mathbf{s}_{k+1} \in C_T^i \ominus G\mathcal{W}. \end{array} \right\}$$

The set C_T^∞ is then computed by $C_T^\infty = \bigcap_{i=0}^\infty C_T^i$, where the initial set is $C_T^0 = C_T$. The recursive computation method can provide the C_T^∞ until $C_T^i = C_T^{i+1}$ [37], [41]. This paper adopts the Multi-parametric toolbox from [42] in MATLAB to compute the set C_T^∞ , as shown in Fig. 4.

In this paper, we additionally consider the soft constraints on the first-step input. Thus, the slack variables, i.e., $\underline{\sigma} \in \mathbb{R}$ and $\bar{\sigma} \in \mathbb{R}$, are used in the cost function given by

$$\mathcal{J}_s = \mathcal{J} + \underline{\sigma}^T S \underline{\sigma} + \bar{\sigma}^T S \bar{\sigma} \quad (45)$$

where $S > 0$. Then, we have the final K-SMPC algorithm such that

$$\mathbf{v}_{\cdot|k}^* = \arg \min_{\mathbf{v}_{k+i|k}} \mathcal{J}_s \quad (46a)$$

subject to

$$\mathbf{s}_{k+i+1|k} = A_{cl} \mathbf{s}_{k+i|k} + B \mathbf{v}_{k+i|k} + B_\varphi \varphi_{k+i|k}, \quad (46b)$$

$$\mathbf{s}_{k+i|k} \in \mathcal{S}, \quad (46c)$$

$$\mathbf{u}_{k+i|k} \in \mathcal{U}, \quad (46d)$$

$$\mathbf{s}_{k+1|k} \in C_T^\infty \ominus G\mathcal{W}, \quad (46e)$$

$$\underline{\mathbf{u}}_s - \underline{\sigma} \leq \mathbf{u}_{k|k} \leq \bar{\mathbf{u}}_s + \bar{\sigma}, \quad (46f)$$

$$0 \leq \underline{\sigma} \leq \underline{\mathbf{u}}_s - \underline{\mathbf{u}}, \quad 0 \leq \bar{\sigma} \leq \bar{\mathbf{u}} - \bar{\mathbf{u}}_s, \quad (46g)$$

$$\mathbf{s}_{k+N|k} \in \mathcal{S}_f, \quad (46h)$$

$$\mathbf{s}_{k|k} = \mathbf{z}_{k|k}, \quad (46i)$$

$$i \in \{0, \dots, N-1\}, \quad (46j)$$

where $\underline{\mathbf{u}}_s \in \mathbb{R}$ and $\bar{\mathbf{u}}_s \in \mathbb{R}$ are the upper and lower bound for the first control input, respectively. In (46f), we can see that the soft constraint is used in the first-step input. We also consider the slack variable to satisfy the input constraint (46d) by imposing (46g).

Remark 3. We impose the input constraint (46d) to consider the physically bounded front tire angle δ of vehicles. In addition, it is needed to minimize the tire angle on straight roads or curved roads with small curvature. To that end, we additionally impose the input constraint (46f) with slack variables, i.e., $\underline{\sigma}$ and $\bar{\sigma}$. \diamond

As mentioned above, the recursive feasibility is guaranteed by the constraint (46e). Moreover, the following theorem provides the details of the recursive feasibility and its proof.

Theorem 2 (Recursive Feasibility [43]). *Let us consider the lifted system (32) with the controller (35). If there exists a feasible solution when $k = 0$, then the optimization problem (46) is feasible for $k > 0$.* \diamond

Proof. If the K-SMPC optimization problem (46) is feasible at $k = 0$, then $\mathbf{s}_{k+1|k} \in C_T^\infty \ominus G\mathcal{W}$. In the next time step, we can obtain $\mathbf{z}_{k+1} = \mathbf{s}_{k+1|k} + G\mathbf{w}_k \in C_T^\infty$ for every realization $\mathbf{w}_k \in \mathcal{W}$, i.e., \mathbf{z}_{k+1} is the feasible state in the next time. Therefore, the K-SMPC optimization problem (46) is recursively feasible. Refer to [43] for more details. \square

In order to prove the stability of the closed-loop system constructed by (46), we introduce a discrete-time Input-to-State Stability (ISS) Lyapunov function [44].

Definition 1 (ISS-Lyapunov function [44]). *A function $V : \mathbb{R}^N \rightarrow \mathbb{R}_+$ is an ISS-Lyapunov function for system $\mathbf{z}_{k+1} = f_L(\mathbf{z}_k, \mu_k)$ if the following holds:*

- There exist \mathcal{K}_∞ functions α_1, α_2 such that

$$\alpha_1(\|\mathbf{z}\|) \leq V(\mathbf{z}) \leq \alpha_2(\|\mathbf{z}\|), \quad \forall \mathbf{z} \in \mathbb{R}^N.$$

- There exist a \mathcal{K}_∞ function α_3 and a \mathcal{K} function γ such that

$$V(f_L(\mathbf{z}, \mu)) - V(\mathbf{z}) \leq -\alpha_3(\|\mathbf{z}\|) + \gamma(\|\mu\|)$$

for all $\mathbf{z} \in \mathbb{R}^N$, and $\mu \in \mathcal{M}$. \diamond

Using Definition 1, the following theorem provides the stability of the closed-loop system.

Theorem 3 (Stability of closed-loop system). *If feasibility of (46) at $k = 0$ is given, then the closed-loop system (46) under the proposed controller is input-to-state stable with the ISS-Lyapunov function*

$$V(\mathbf{z}_k^*) = \mathbb{E} \left\{ \sum_{i=0}^{N_p-1} (\|\mathbf{z}_{k+i|k}^*\|_Q^2 + \|\mathbf{u}_{k+i|k}^*\|_R^2) + \|\mathbf{z}_{k+N_p|k}^*\|_P^2 \right\}.$$

\diamond

Proof. Let $V(\mathbf{z}_k^*)$ and $V(\mathbf{z}_{k+1}^*)$ be an ISS-Lyapunov candidate function at time k and $k+1$, respectively. With the stabilizing control input after prediction horizon $\mathbf{u}_{k+N|k} = K\mathbf{z}_{k+N|k}$, we have

$$\begin{aligned} & \mathbb{E}\{V(\mathbf{z}_{k+1}^*)\} - V(\mathbf{z}_k^*) \\ &= \mathbb{E} \left\{ \sum_{i=1}^{N_p-1} (\|\mathbf{z}_{k+i|k}^*\|_Q^2 + \|\mathbf{u}_{k+i|k}^*\|_R^2) + \|\mathbf{z}_{k+N_p|k}^*\|_P^2 \right. \\ & \quad \left. + \|\mathbf{u}_{k+N_p|k}^*\|_R^2 + \|\mathbf{z}_{k+N_p+1|k}^*\|_P^2 \right\} - V(\mathbf{z}_k^*) \\ &\leq \mathbb{E} \left\{ \|\mathbf{z}_{k+N_p|k}^*\|_Q^2 + \|\mathbf{z}_{k+N_p|k}^*\|_{K^T R K}^2 + \|\mathbf{z}_{k+N_p|k}^*\|_{A_{cl}^T P A_{cl}}^2 \right. \\ & \quad \left. + \|B_\varphi \varphi_{k+N_p|k}\|_P^2 + \|G\mathbf{w}_{k+N_p|k}\|_P^2 - \|\mathbf{z}_{k|k}^*\|_Q^2 - \|\mathbf{u}_{k|k}^*\|_R^2 \right. \\ & \quad \left. - \|\mathbf{z}_{k+N_p|k}^*\|_P^2 \right\} \\ &= \mathbb{E} \left\{ -\|\mathbf{z}_{k|k}^*\|_Q^2 - \|\mathbf{u}_{k|k}^*\|_R^2 + \|B_\varphi \varphi_{k+N_p|k}\|_P^2 \right. \\ & \quad \left. + \|G\mathbf{w}_{k+N_p|k}\|_P^2 \right\} \\ &\leq -\|\mathbf{z}_{k|k}^*\|_Q^2 + \|B_\varphi \varphi_{k+N_p|k}\|_P^2 + \mathbb{E} \left\{ \|G\mathbf{w}_{k+N_p|k}\|_P^2 \right\} \end{aligned} \quad (47)$$

where $\mathbf{s}_{k|k}^* = \mathbf{z}_{k|k}^*$, and $A_{cl}^T P A_{cl} + K^T R K + Q = P$ since P is the solution of (34). Therefore, $V(\mathbf{z}_k^*)$ is the ISS-Lyapunov function and the closed-loop system is input-to-state stable. \square

Moreover, summing (47) over $k = 0, 1, \dots$ leads to

$$\lim_{n \rightarrow \infty} \frac{1}{n} \sum_{k=0}^n \mathbb{E}(\|\mathbf{z}_k\|_Q^2 + \|\mathbf{u}_k\|_R^2) \leq L_{ss} \quad (48)$$

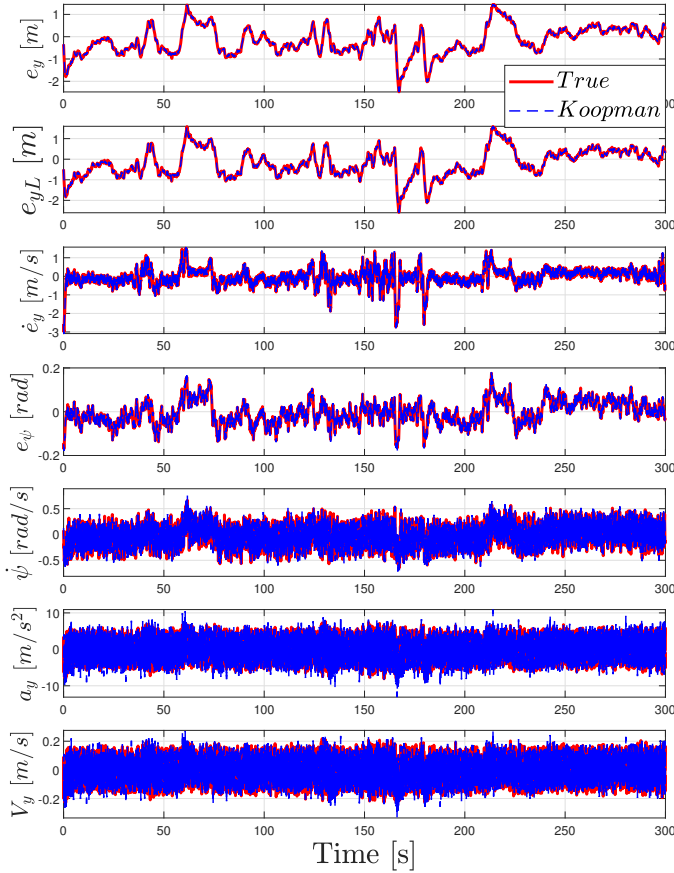


Fig. 5. Model fitting accuracy of the Koopman model with validation set

where $L_{ss} = \lim_{n \rightarrow \infty} \sum_{k=0}^n \mathbb{E}(\|B_\varphi \varphi_k\|_P^2 + \|G \mathbf{w}_k\|_P^2) / n$ by using discrete-time version of Dynkin's Formula [45]. It is straightforward that the state of the closed-loop system does not converge asymptotically to the origin but remains within a neighborhood of the origin due to the external signal and uncertainty by viewing (48), which means mean-square stability [23], [38].

V. SIMULATION RESULTS

A. Simulation Set-up and Koopman Operator-based Vehicle Modeling

The proposed method was validated using the co-simulation platform with MATLAB/Simulink and CarSim. The vehicle dynamic simulator, CarSim, provides a vehicle model with 27 degrees of freedom for representing the highly nonlinear vehicle dynamics allowing for testing of the realistic motion of a vehicle. We used various roads provided by CarSim to obtain the training dataset for computing the Koopman operator with a sample time of 0.01s. Some of the system states are related to the given road lane, i.e., e_y , e_{yL} , \dot{e}_y , and e_ψ ; thus a path-follow controller stabilizing the vehicle lateral motion is needed to obtain the dataset. Moreover, random signals are added to the input to sufficiently excite the nonlinear vehicle dynamics. For more details, please refer to our previous work [25], [30]. Then, the dataset matrices (28) is obtained with $M = 1.22 \times 10^5$. We chose $N = 22$ in (26) to obtain the lifted state.

In addition, it is reported that a thin plate spline radial basis function is an effective lifting function in autonomous vehicle modeling compared to the other basis functions [25]. Thus, the nonlinear lifting functions ϕ_i are selected as the thin plate spline radial basis functions, i.e., $\phi_i(\mathbf{x}) = \|\mathbf{x} - \mathbf{c}_i\|_2^2 \cdot \log\|\mathbf{x} - \mathbf{c}_i\|_2$ where \mathbf{c}_i is randomly selected with a uniform distribution in a certain range [18]. The number of thin plate spline radial basis functions is set to 15 in (29).

Based on the obtained training dataset, we approximate the Koopman operator in the finite-dimensional space using (31). The approximated Koopman operator is tested to validate the modeling accuracy with a validation dataset. The fitting performance is shown in Fig. 5. The red line depicts the true state of the vehicle acquired from CarSim, and the blue line illustrates the predicted vehicle state by the Koopman operator-based vehicle model. As shown in Fig. 5, the Koopman-based vehicle model can predict the vehicle state well.

B. Comparative Study

In order to conduct a comparative study, we adopted two methods, the L-SMPC and the K-LQ. The details of each method are as follows:

- L-SMPC: The linear vehicle model was adopted as the look-ahead lateral dynamic model from [2], [29] given by

$$\dot{\mathbf{x}}_v = A_v \mathbf{x}_v + B_v \mathbf{u}_v + B_{v\varphi} \varphi_v, \quad (49)$$

where

$$A_v = \begin{bmatrix} 0 & 1 & 0 & -L \\ 0 & a_{22} & a_{23} & a'_{24} \\ 0 & 0 & 0 & -1 \\ 0 & a'_{42} & a_{43} & a_{44} \end{bmatrix}, \quad B_v = \begin{bmatrix} 0 \\ b'_{21} \\ 0 \\ b_{41} \end{bmatrix},$$

$$B_{v\varphi} = \begin{bmatrix} L & V_x \\ V_x & 0 \\ 1 & 0 \\ 0 & 0 \end{bmatrix}, \quad \mathbf{u}_v = \delta, \quad \varphi_v = \begin{bmatrix} \dot{\psi}_{des} \\ e_{\psi L} - e_\psi \end{bmatrix},$$

with

$$a_{22} = -\frac{2C_{\alpha f} + 2C_{\alpha r}}{mV_x}, \quad a_{23} = -a_{22}V_x,$$

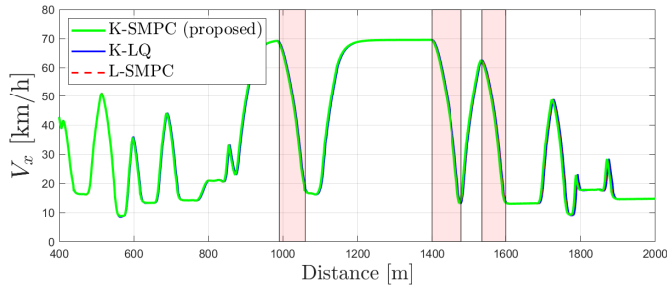
$$a_{24} = -1 - \frac{2C_{\alpha f}l_f - 2C_{\alpha r}l_r}{mV_x^2}, \quad a'_{24} = (a_{24} - 1)V_x,$$

$$a_{42} = -\frac{2C_{\alpha f}l_f - 2C_{\alpha r}l_r}{I_z}, \quad a'_{42} = a_{42}/V_x,$$

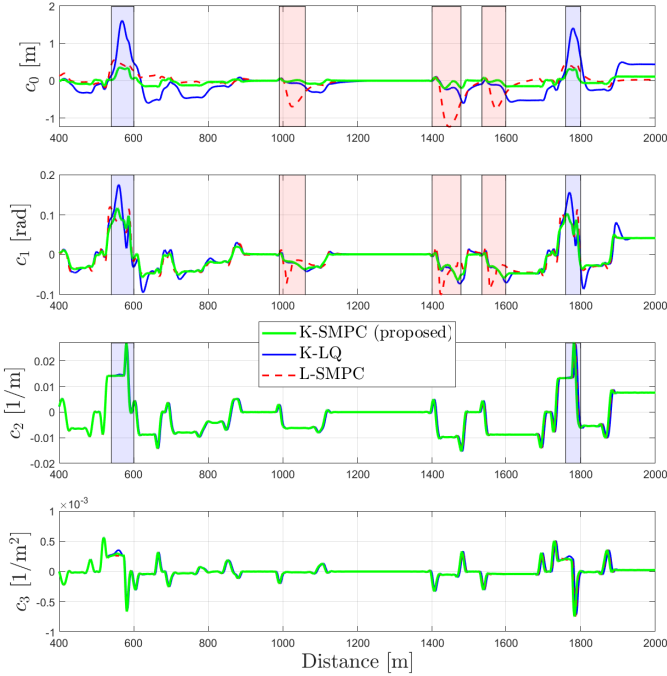
$$a_{43} = -a_{42}, \quad a_{44} = -\frac{2C_{\alpha f}l_f^2 + 2C_{\alpha r}l_r^2}{I_z V_x},$$

$$b_{21} = \frac{2C_{\alpha f}}{mV_x}, \quad b'_{21} = b_{21}V_x, \quad b_{41} = \frac{2C_{\alpha f}l_f}{I_z}.$$

Then, the linear vehicle model was discretized with the zero-order-holder method. We designed the SMPC to be similar to (46) except for the system model (46b). The linear model-based SMPC for the LKS was successfully studied in [46]. However, the linear model is not appropriate since the cornering stiffness is no longer linear with respect to the tire slip angle when the road curvature is high and vehicle speed rapidly changes [5], [46]. Therefore, we can confirm the effectiveness of the



(a) V_x



(b) C_0 , C_1 , C_2 , and C_3

Fig. 6. L-SMPC has large tracking error (C_0 and C_1) in pink-colored section, where vehicle speed is rapidly varying. K-LQ has large tracking error (C_0 and C_1) in blue-colored section, where road has high curvature: (a) Vehicle longitudinal speed, and (b) road coefficients.

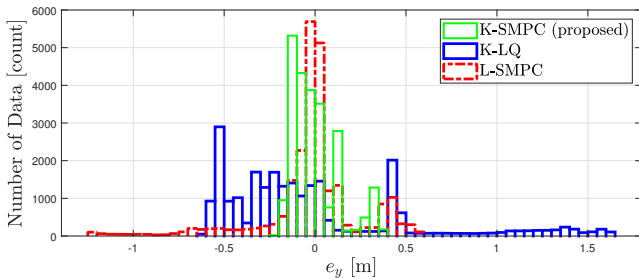
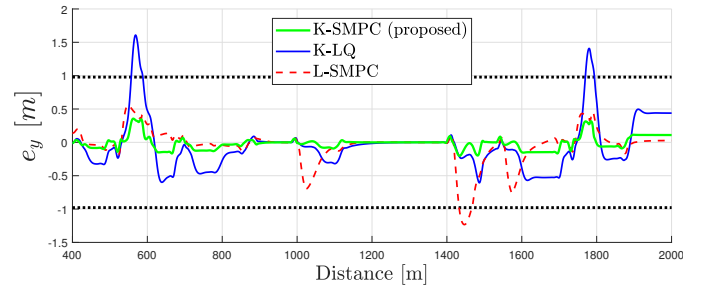


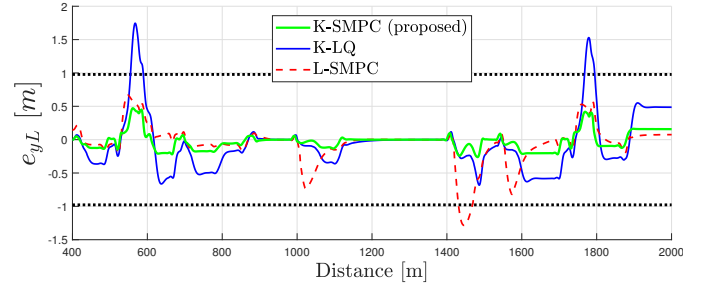
Fig. 7. e_y histogram

proposed method in dynamic lane-keeping scenarios by comparing the result of the L-SMPC.

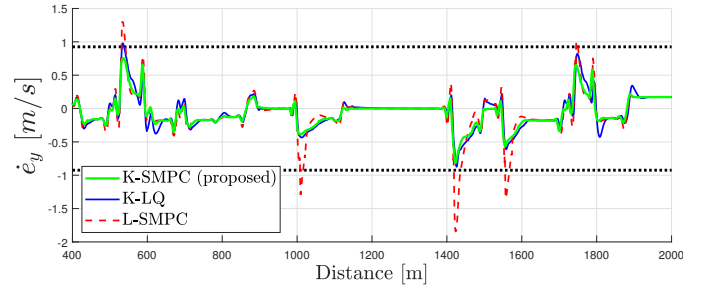
- K-LQ [25]: The K-LQ method uses the Koopman operator-based vehicle model, the same as (32). However,



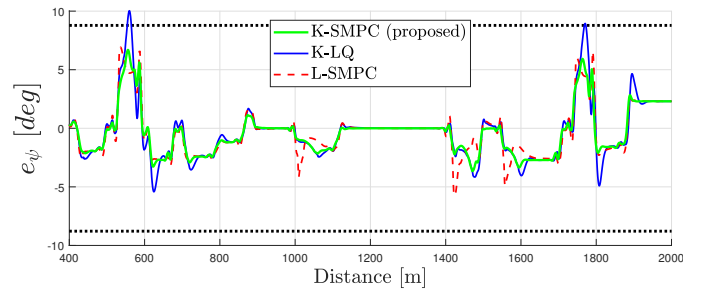
(a) Lateral position error w.r.t. lane, e_y



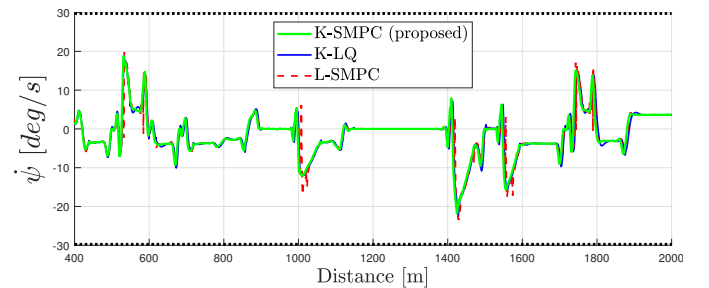
(b) Lateral position error on the look-ahead point, e_{yL}



(c) Derivative of the lateral position error, \dot{e}_y



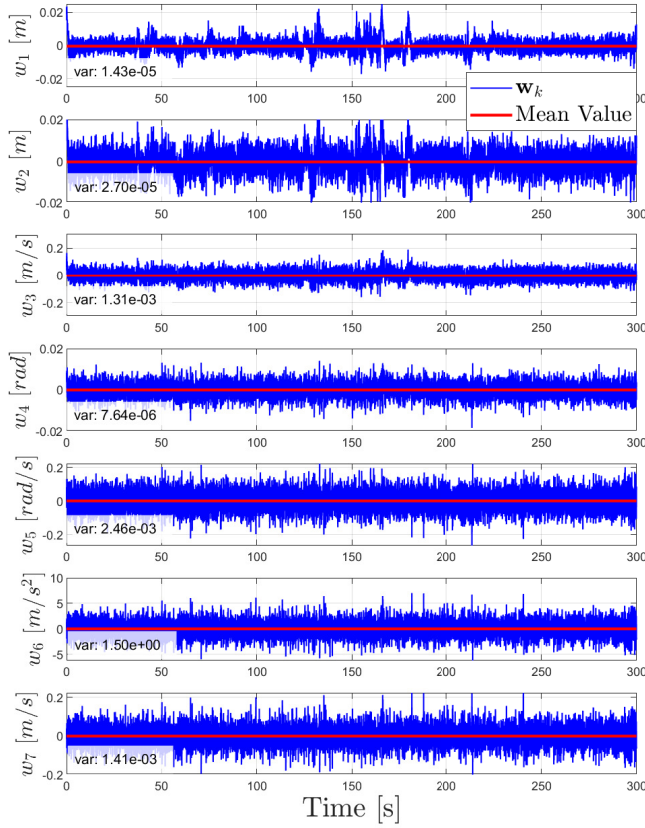
(d) Heading angle error w.r.t. lane, e_ψ



(e) Yaw-rate of the vehicle, $\dot{\psi}$

Fig. 8. Control results of the system state

the linear quadratic regulator was adopted to control the system, i.e., the only difference with the proposed method is the control scheme. From [25], the road information,


 Fig. 9. Uncertainty w_k for each system state

i.e., φ , was not considered in the controller design. Thus, we can evaluate the tracking performance of the proposed scheme on high-curvature roads by comparing the performance of the K-LQ.

For fair comparison with the proposed method, we used the same weighting matrix on the system state and control input in the design of the controller of each method. Moreover, this paper designs the longitudinal controller to control the vehicle speed with respect to the road curvature with a proportional-derivative (PD) controller. The design process of the longitudinal controller is out of the scope of this paper; hence, the reader can refer to the authors' work [47] for a detailed description. In Fig. 6 (a), it can be shown that the vehicle longitudinal speed is equal to each method. Thus, the tracking performance of each method only depends on each lateral controller.

We use the race-track road provided by CarSim to validate the tracking performance of each method. The road lane coefficients, i.e., C_0 , C_1 , C_2 , and C_3 in (2), are illustrated in Fig. 6 (b). The blue line represents the result of the K-LQ, the red line is the L-SMPC, and the green line depicts the result of the proposed method. It should be noted that C_2 is the curvature of the lane, representing the road shape. Hence, each control method was conducted on the same path. As mentioned in II-A, C_0 denotes the lateral offset error, and C_1 denotes the heading angle error. We can see that

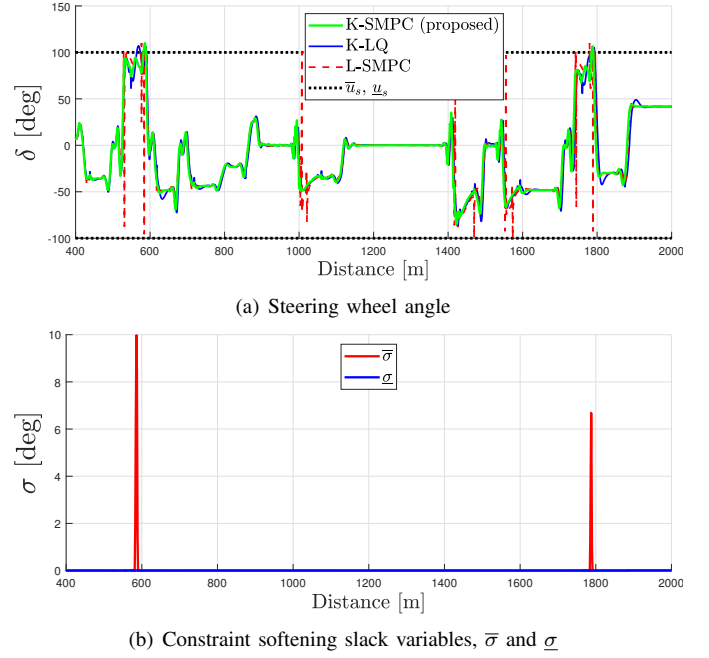


Fig. 10. Results of control input and slack variables

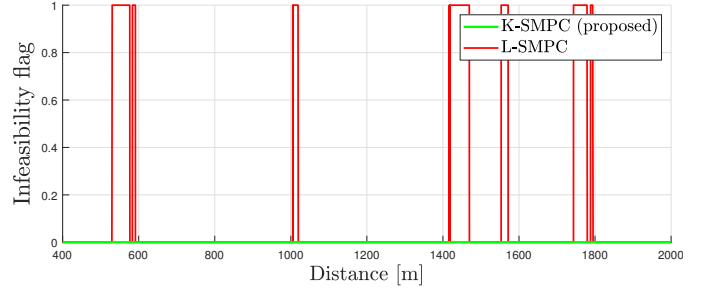


Fig. 11. SMPC infeasibility: 0 for feasible, 1 for infeasible

the proposed method has a lower lateral position error and a lower heading angle error, i.e., C_0 and C_1 , compared to other methods in Fig. 6 (b). In particular, the proposed controller had a lower error on the lane with a high curvature, as shown by the blue section in Fig. 6 (b). However, the L-SMPC had a large error in the pink section in Fig. 6 (b) compared to other methods because the linear vehicle model is no longer accurate with rapid varying of vehicle speed [5], as illustrated by the pink section in Fig. 6 (a). On the other hand, the K-LQ can track the given lane even with rapid speed changes because the Koopman operator-based vehicle model can represent the highly nonlinear vehicle dynamics. However, the K-LQ has a larger error on roads with a high curvature, as depicted by the blue region in Fig. 6 (b). This is because the K-LQ does not consider the future system state, while the K-SMPC and the L-SMPC predict the future state with the curved road information from φ in the optimization problem. As mentioned before, C_0 denotes the lateral offset error, which is equal to the system state e_y . Thus, we observe that the proposed method has the lowest lateral error by the statistical way, i.e., histogram, as is shown in Fig. 7.

The results of the controlled system state are observed in

Fig. 8. As defined by the state of the system in (22), some states represent the path-tracking performance. Specifically, e_y and e_{yL} are the lateral position errors at CG and the look-ahead distance, respectively. In addition, \dot{e}_y is the lateral speed tracking error, and e_ψ is the heading angle tracking error. In Fig. 8, the blue line represents the K-LQ, the red line represents the L-SMPC result, the green line represents the proposed method, and the black line represents the tightened constraints of each state. We set the constraints as $|e_y| \leq 1$ m, $|e_{yL}| \leq 1$ m, $|\dot{e}_y| \leq 0.95$ m/s, $|e_{psi}| \leq 10$ deg, and $|\dot{\psi}| \leq 30$ deg/s, respectively. Besides, we set the covariance matrix Σ_w from the data. The uncertainty \mathbf{w}_k is computed, as shown in Fig. 9. We calculate the variance for each state, then we use the variance for design the covariance matrix. The covariance matrix is defined as $\Sigma_w = \text{diag}[\sigma_1 \ \sigma_2 \ \sigma_3 \ \sigma_4 \ \sigma_5 \ \sigma_6 \ \sigma_7 \ \mathbf{0}_{1 \times (N-7)}]$ where $\sigma_1 = 1.43e-5$, $\sigma_2 = 2.70e-5$, $\sigma_3 = 1.31e-3$, $\sigma_4 = 7.64e-6$, $\sigma_5 = 2.46e-3$, $\sigma_6 = 1.5$, and $\sigma_7 = 1.41e-3$. As shown in Fig. 8, it can be observed that the proposed method has less error in the lateral position, lateral speed, and heading angle, i.e., e_y , e_{yL} , \dot{e}_y , and e_ψ . Moreover, the proposed controller satisfies the given constraints of each system state, while other methods violate the constraints in some sections. As a result, the proposed method has better tracking performance than the other methods in the LKS application. We can observe the quantitative results in Table. I and Table. II. It can be confirmed that the lateral position error is dramatically reduced with the proposed method.

In Fig. 10 (a), the control inputs of each method are depicted. The result of the K-LQ is the blue line, the L-SMPC method is the red line, the K-SMPC is the green line, and the first step input constraints are shown as the black line. It can be seen that the L-SMPC has a large oscillation in some ranges because the L-SMPC is infeasible where the given constraints are violated, as shown in Fig. 11. On the other hand, the K-LQ and the K-SMPC method have a smooth control input. In addition, we can observe that the proposed method slightly violates the input constraints at about 600 m and 1800 m to control the vehicle on the high curvature road. However, note

TABLE I
COMPARISON OF CONTROLLER PERFORMANCE ON VALIDATION ROAD

State	Root Mean Squared Error				
	e_y	e_{yL}	\dot{e}_y	e_ψ	$\dot{\psi}$
K-LQ	0.517	0.571	0.252	0.055	0.088
L-SMPC	0.266	0.299	0.271	0.043	0.089
K-SMPC	0.130	0.180	0.220	0.045	0.088

TABLE II
COMPARISON OF CONTROLLER PERFORMANCE ON VALIDATION ROAD

State	Max Error				
	e_y	e_{yL}	\dot{e}_y	e_ψ	$\dot{\psi}$
K-LQ	1.608	1.746	0.978	0.175	0.396
L-SMPC	1.233	1.285	1.845	0.121	0.410
K-SMPC	0.356	0.472	0.817	0.117	0.381

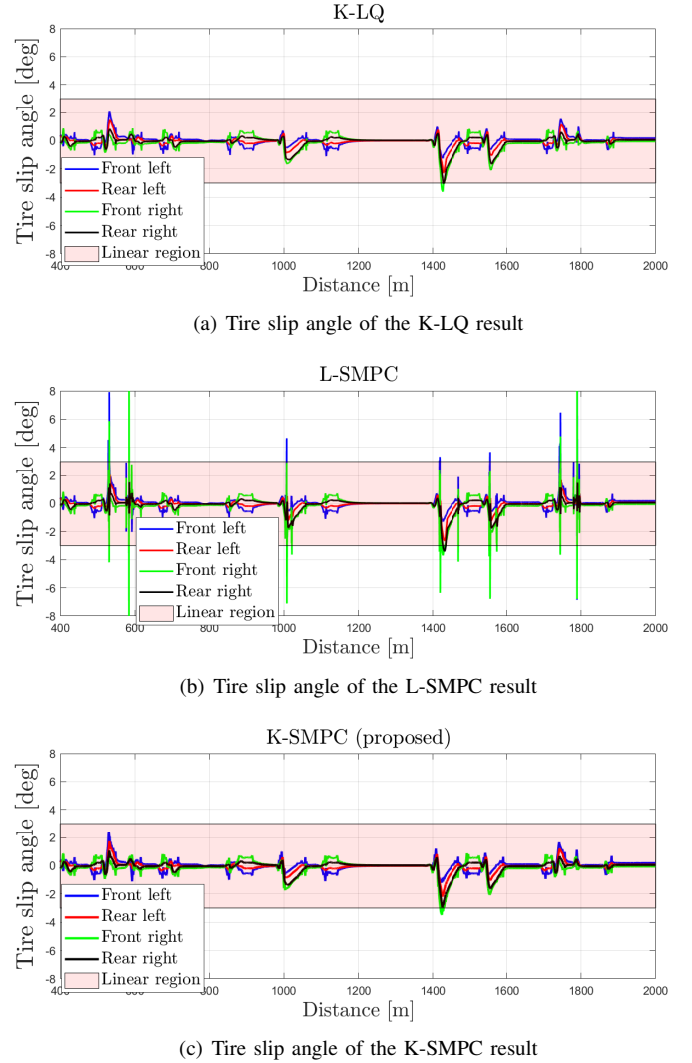


Fig. 12. Results of the tire slip angle

that we consider the soft constraints on the first step of the input. Thus, the slack variables can be observed, as shown in Fig. 10 (b).

The results of each tire slip angle are shown in Fig. 12 for each method. The pink section of Fig. 12 represents the linear relationship between the lateral tire force and the tire slip angle [5], [25], i.e., the cornering stiffness is a linear function of the tire slip angle in (5). In this paper, the linear region is selected within ± 3 deg of the tire slip angle because the lateral tire force and the tire slip angle can be in a linear relationship provided by CarSim data and references [5], [25]. The Koopman-based vehicle model (i.e., K-LQ and K-SMPC) maintains the tire slip in the linear region. Thus, it can be seen that the Koopman-based model captures the vehicle's nonlinear behavior and effectively controls the vehicle under dynamic situations. On the other hand, the L-SMPC method leaves the linear region so that the linear vehicle model is no longer valid.

VI. CONCLUSION

In this paper, we proposed the K-SMPC for the enhanced LKS of autonomous vehicles. The EDMD method was used to approximate the Koopman operator in a finite-dimensional space for practical implementation. We considered the modeling error of the approximated Koopman operator in the EDMD method. The modeling error was handled as a probabilistic signal. Then, we designed K-SMPC to tackle the modeling error. The recursive feasibility of the proposed method was guaranteed with the explicit first-step state constraint by computing the robust control invariant set. For the simulation, a high-fidelity vehicle simulator, CarSim, was used to validate the effectiveness of the K-SMPC. We conducted a comparative study between K-LQ and L-SMPC. From the results, it was confirmed that the proposed method outperforms other methods with respect to the tracking performance. Furthermore, we observed that the proposed method satisfies the given constraints and is recursively feasible. As future work, a comparative study will be conducted with the Koopman-based RMPC to evaluate the conservativeness quantitatively. Future research may also include a real-car experiment with the proposed method.

REFERENCES

- [1] J. W. Seo, D. J. Kim, J. S. Kim, and C. C. Chung, "LPV H2 state feedback controller for automated parking system," *IEEE Control Systems Letters*, vol. 6, pp. 572–577, 2021.
- [2] Y. S. Quan, J. S. Kim, and C. C. Chung, "Linear parameter varying models-based gain-scheduling control for lane keeping system with parameter reduction," *IEEE Transactions on Intelligent Transportation Systems*, vol. 23, no. 11, pp. 20746–20756, 2022.
- [3] W. Y. Choi, S.-H. Lee, and C. C. Chung, "Horizon-wise model predictive control with application to autonomous driving vehicle," *IEEE Transactions on Industrial Informatics*, vol. 18, no. 10, pp. 6940–6949, 2022.
- [4] J. S. Kim, S.-H. Lee, and C. C. Chung, "Lane change control with optimal time-varying sliding mode in automated driving vehicle," in *2020 American Control Conference (ACC)*. IEEE, 2020, pp. 430–435.
- [5] R. Rajamani, *Vehicle dynamics and control*. Springer Science & Business Media, 2011.
- [6] S. W. Kim, Y. W. Jeong, J. S. Kim, S.-H. Lee, and C. C. Chung, "Vehicular vertical tire forces estimation using unscented kalman filter," in *2019 Asian Control Conference (ASCC)*. IEEE, 2019, pp. 325–330.
- [7] S. L. Brunton and J. N. Kutz, *Data-driven science and engineering: Machine learning, dynamical systems, and control*. Cambridge University Press, 2022.
- [8] S. L. Brunton, J. L. Proctor, and J. N. Kutz, "Discovering governing equations from data by sparse identification of nonlinear dynamical systems," *Proceedings of the national academy of sciences*, vol. 113, no. 15, pp. 3932–3937, 2016.
- [9] B. O. Koopman, "Hamiltonian systems and transformation in hilbert space," *Proceedings of the national academy of sciences of the united states of america*, vol. 17, no. 5, p. 315, 1931.
- [10] V. Cibulka, T. Haniš, and M. Hromčík, "Data-driven identification of vehicle dynamics using koopman operator," in *2019 International Conference on Process Control (PC19)*. IEEE, 2019, pp. 167–172.
- [11] Y. Xiao, X. Zhang, X. Xu, X. Liu, and J. Liu, "Deep neural networks with koopman operators for modeling and control of autonomous vehicles," *IEEE Transactions on Intelligent Vehicles*, vol. 8, no. 1, pp. 135–146, 2022.
- [12] M. Švec, Š. Ileš, and J. Matuško, "Model predictive control of vehicle dynamics based on the koopman operator with extended dynamic mode decomposition," in *2021 IEEE International Conference on Industrial Technology (ICIT)*. IEEE, 2021, pp. 68–73.
- [13] V. Cibulka, T. Haniš, M. Korda, and M. Hromčík, "Model predictive control of a vehicle using koopman operator," *IFAC-PapersOnLine*, vol. 53, no. 2, pp. 4228–4233, 2020.
- [14] M. Švec, Š. Ileš, and J. Matuško, "Predictive approach to torque vectoring based on the koopman operator," in *2021 European Control Conference (ECC)*. IEEE, 2021, pp. 1341–1346.
- [15] S. Yu, C. Shen, and T. Eرسال, "Autonomous driving using linear model predictive control with a koopman operator based bilinear vehicle model," *IFAC-PapersOnLine*, vol. 55, no. 24, pp. 254–259, 2022.
- [16] Y. Xiao, X. Zhang, X. Xu, Y. Lu, and J. Lil, "DDK: A deep koopman approach for longitudinal and lateral control of autonomous ground vehicles," in *2023 IEEE International Conference on Robotics and Automation (ICRA)*. IEEE, 2023, pp. 975–981.
- [17] R. Wang, Y. Han, and U. Vaidya, "Deep koopman data-driven control framework for autonomous racing," in *International Conference on Robotics and Automation (ICRA) Workshop Opportunities Challenges Auton. Racing*, 2021, pp. 1–6.
- [18] M. Korda and I. Mezić, "Linear predictors for nonlinear dynamical systems: Koopman operator meets model predictive control," *Automatica*, vol. 93, pp. 149–160, 2018.
- [19] X. Zhang, W. Pan, R. Scattolini, S. Yu, and X. Xu, "Robust tube-based model predictive control with koopman operators," *Automatica*, vol. 137, p. 110114, 2022.
- [20] J. S. Kim, Y. S. Quan, and C. C. Chung, "Uncertainty quantification of autoencoder-based koopman operator," *arXiv preprint arXiv:2309.09419*, 2023.
- [21] S. H. Son, A. Narasingam, and J. S.-I. Kwon, "Handling plant-model mismatch in koopman lyapunov-based model predictive control via offset-free control framework," *arXiv preprint arXiv:2010.07239*, 2020.
- [22] Y. Wang, Y. Yang, Y. Pu, and C. Manzie, "Data-driven predictive tracking control based on koopman operators," *arXiv preprint arXiv:2208.12000*, 2022.
- [23] M. Farina, L. Giulioni, and R. Scattolini, "Stochastic linear model predictive control with chance constraints—a review," *Journal of Process Control*, vol. 44, pp. 53–67, 2016.
- [24] A. Mesbah, "Stochastic model predictive control: An overview and perspectives for future research," *IEEE Control Systems Magazine*, vol. 36, no. 6, pp. 30–44, 2016.
- [25] J. S. Kim, Y. S. Quan, and C. C. Chung, "Koopman operator-based model identification and control for automated driving vehicle," *International Journal of Control, Automation and Systems*, vol. 21, no. 8, pp. 2431–2443, 2023.
- [26] S.-H. Lee and C. C. Chung, "Autonomous-driving vehicle control with composite velocity profile planning," *IEEE Transactions on Control Systems Technology*, vol. 29, no. 5, pp. 2079–2091, 2020.
- [27] E. D. Dickmanns and A. Zapp, "A curvature-based scheme for improving road vehicle guidance by computer vision," in *Mobile Robots I*, vol. 727. SPIE, 1987, pp. 161–168.
- [28] W. Y. Choi, S.-H. Lee, and C. C. Chung, "Robust vehicular lane-tracking control with a winding road disturbance compensator," *IEEE Transactions on Industrial Informatics*, vol. 17, no. 9, pp. 6125–6133, 2020.
- [29] S.-H. Lee and C. C. Chung, "Robust multirate on-road vehicle localization for autonomous highway driving vehicles," *IEEE Transactions on Control Systems Technology*, vol. 25, no. 2, pp. 577–589, 2016.
- [30] J. S. Kim, Y. S. Quan, and C. C. Chung, "Data-driven modeling and control for lane keeping system of automated driving vehicles: Koopman operator approach," in *2022 International Conference on Control, Automation and Systems (ICCAS)*. IEEE, 2022, pp. 1049–1055.
- [31] A. Mauroy, Y. Susuki, and I. Mezić, *Koopman operator in systems and control*. Springer, 2020.
- [32] J. L. Proctor, S. L. Brunton, and J. N. Kutz, "Generalizing koopman theory to allow for inputs and control," *SIAM Journal on Applied Dynamical Systems*, vol. 17, no. 1, pp. 909–930, 2018.
- [33] M. O. Williams, M. S. Hemati, S. T. Dawson, I. G. Kevrekidis, and C. W. Rowley, "Extending data-driven koopman analysis to actuated systems," *IFAC-PapersOnLine*, vol. 49, no. 18, pp. 704–709, 2016.
- [34] M. O. Williams, I. G. Kevrekidis, and C. W. Rowley, "A data-driven approximation of the koopman operator: Extending dynamic mode decomposition," *Journal of Nonlinear Science*, vol. 25, no. 6, pp. 1307–1346, 2015.
- [35] Y. S. Son, W. Kim, S.-H. Lee, and C. C. Chung, "Robust multirate control scheme with predictive virtual lanes for lane-keeping system of autonomous highway driving," *IEEE Transactions on Vehicular Technology*, vol. 64, no. 8, pp. 3378–3391, 2014.
- [36] A. W. Marshall and I. Olkin, "Multivariate chebyshev inequalities," *The Annals of Mathematical Statistics*, pp. 1001–1014, 1960.

- [37] M. Lorenzen, F. Dabbene, R. Tempo, and F. Allgöwer, "Constraint-tightening and stability in stochastic model predictive control," *IEEE Transactions on Automatic Control*, vol. 62, no. 7, pp. 3165–3177, 2016.
- [38] B. Kouvaritakis, M. Cannon, S. V. Raković, and Q. Cheng, "Explicit use of probabilistic distributions in linear predictive control," *Automatica*, vol. 46, no. 10, pp. 1719–1724, 2010.
- [39] M. Korda, R. Gondhalekar, J. Cigler, and F. Oldewurtel, "Strongly feasible stochastic model predictive control," in *2011 50th IEEE Conference on Decision and Control and European Control Conference*. IEEE, 2011, pp. 1245–1251.
- [40] P.-O. Gutman and M. Cwikel, "An algorithm to find maximal state constraint sets for discrete-time linear dynamical systems with bounded controls and states," *IEEE Transactions on Automatic Control*, vol. 32, no. 3, pp. 251–254, 1987.
- [41] F. Blanchini and S. Miani, *Set-theoretic methods in control*. Springer, 2008, vol. 78.
- [42] M. Herceg, M. Kvasnica, C. N. Jones, and M. Morari, "Multi-parametric toolbox 3.0," in *2013 European control conference (ECC)*. IEEE, 2013, pp. 502–510.
- [43] M. Lorenzen, F. Allgöwer, F. Dabbene, and R. Tempo, "An improved constraint-tightening approach for stochastic mpc," in *2015 American Control Conference (ACC)*. IEEE, 2015, pp. 944–949.
- [44] Z.-P. Jiang and Y. Wang, "Input-to-state stability for discrete-time nonlinear systems," *Automatica*, vol. 37, no. 6, pp. 857–869, 2001.
- [45] H. J. Kushner and Kushner, *Stochastic stability and control*. Academic press New York, 1967, vol. 33.
- [46] C. Zhang, C. Zhuang, X. Zheng, R. Cai, and M. Li, "Stochastic model predictive control approach to autonomous vehicle lane keeping," *Journal of Shanghai Jiaotong University (Science)*, vol. 26, pp. 626–633, 2021.
- [47] Y. S. Quan, J. S. Kim, and C. C. Chung, "Robust control for lane keeping system using a linear parameter varying approach with scheduling variables reduction," *International Journal of Control, Automation and Systems*, vol. 20, no. 7, pp. 2097–2106, 2022.



Jin Sung Kim (Graduate Student Member, IEEE) received his B.S. degree in electronic engineering from Kookmin University, Seoul, South Korea, in 2014, and M.S. degree in electrical engineering from Hanyang University, Seoul, in 2019, where he is currently pursuing his Ph.D. degree in electrical engineering. His main research interests include data-driven control, automated vehicles, optimal control, robust control, and artificial intelligence. Jin Sung Kim received the Outstanding Student Paper Award at International Conference on Control, Automation

and Systems in 2022. He is a member of the IEEE INTELLIGENT TRANSPORTATION SYSTEMS SOCIETY (ITSS), IEEE CONTROL SYSTEM SOCIETY (CSS), the SOCIETY OF AUTOMOTIVE ENGINEERS (SAE), the KOREAN SOCIETY OF AUTOMOTIVE ENGINEERS (KSAE), and the INSTITUTE OF CONTROL, ROBOTICS AND SYSTEMS (ICROS).



Ying Shuai Quan (Graduate Student Member, IEEE) received a B.S. degree in control science and engineering in 2017 from the School of Astronautics, Harbin Institute of Technology, Harbin, China. She is working towards her Ph.D. in the Systems and Control Laboratory at the electrical engineering College of Engineering, Hanyang University, Seoul, Korea. Her main research interests include optimal control and learning-based control for autonomous systems. She is a student member of the KOREAN SOCIETY OF AUTOMOTIVE ENGINEERS (KSAE)

and the INSTITUTE OF CONTROL, ROBOTICS, AND SYSTEMS (ICROS).



Chung Choo Chung received his B.S. and M.S. degrees in electrical engineering from Seoul National University, Seoul, South Korea, and his Ph.D. degree in electrical and computer engineering from the University of Southern California, Los Angeles, CA, USA, in 1993. From 1994 to 1997, he was with the Samsung Advanced Institute of Technology, South Korea. In 1997, he joined the Faculty of Hanyang University, Seoul, South Korea. Dr. Chung was an Associate Editor for the *Asian Journal of Control* from 2000 to 2002 and an (Founding) Editor

for the *International Journal of Control, Automation and Systems* from 2003 to 2005. He served as associate editor for various international conferences, such as the IEEE CONFERENCE ON DECISION AND CONTROL (CDC), the American Control Conferences, the IEEE Intelligent Vehicles Symposium, and the Intelligent Transportation Systems Conference. He was a guest editor for a special issue on advanced servo control for emerging data storage systems published by the IEEE TRANSACTIONS ON CONTROL SYSTEM TECHNOLOGIES (TCST), 2012 and also a guest editor for the *IEEE Intelligent Transportation Systems Magazine*, 2017. He is currently an associate editor for the *IFAC Mechatronics*. He was a program co-chair of ICCAS-SICE 2009, Fukuoka, Japan, an organizing chair for the INTERNATIONAL CONFERENCE ON CONTROL, AUTOMATION AND SYSTEMS (ICCAS) 2011, KINTEX, Korea and a program co-chair of the 2015 IEEE INTELLIGENT VEHICLES SYMPOSIUM, COEX, Korea. He was the general chair of ICCAS 2019, Jeju, Korea, and the 2019 President of the Institute of Control, Robotics and Systems (ICROS), Korea. He was also a general chair of CDC 2020, held in Jeju, Korea. He is a member of the National Academy of Engineering of Korea (NAEK).